Stress and Displacement Estimates for Arches

Clive L. Dym, F.ASCE[1]; and Harry E. Williams[2]

Abstract: This paper presents analytical estimates of the behavior exhibited by curved, archlike structures under radially directed and gravitational line loads. The behavior is shown to range from elementary beam bending at one end to a state of pure compression at the other, and its behavior can be tracked by an arch rise parameter that is a function of the arch's semivertex angle, radius and thickness. The principal results are useful estimates of the dependence of the major displacements and stress resultants on the arch rise parameter. The results also offer some insight into the assumptions underlying Robert Maillart's arch designs.

DOI: 10.1061/(ASCE)ST.1943-541X.0000267

CE Database subject headings: Arches; Load factors; Stress; Displacement.

Author keywords: Arch structures; Qualitative behavior; Gravity loads; Radially directed loads.

Introduction

Historically, "true" arches are masonry structures such as Roman bridges and arches whose basic elements are the stones of which the arch is constructed. The dominant, and perhaps only, stress state is one of uniform compression (Heyman 1995). On the other hand, structures such as Robert Maillart's beautiful bridges (Billington 1979) are perhaps better characterized as "archlike" structures whose static response is governed not only by their extensional stiffness ($\sim EA/R$), but also by their bending stiffness ($\sim EI/R^3$). Billington (1979) described Maillart's famed Salginatobel bridge (Fig. 1) as "one of the most beautiful examples of pure twentieth-century structure . . . even to the skilled engineer, an object of mystery and wonder," and noted that Maillart's "bridge calculations employed elementary mathematics with no calculus at all" to produce a form that without precedent expressed "one of the simplest of all technical ideas:" a simple arch acting in pure compression. This elegant structural concept formed the basis of Maillart's work, as well of the bridges designed by many others; for example, Christian Menn.

Indeed, while it is "well known" that beams bend and that arches act largely in compression, it is not always obvious how an arch structure behaves or which stresses are dominant, especially to students and engineers inexperienced in the design of bridges or thin shell structures. Furthermore, neither the professional structural engineering literature nor standard structural mechanics textbooks appear to provide much guidance about how variation in arch behavior follows from variations in arch geometry. That is, a review of the standard structures textbooks has failed to produce even a single discussion of how or when a shallow curved beam transitions to an arch, or why arch analyses are presented in terms of the structure's bending stiffness (i.e., EI/R^3) when such arches are presumed to be in compression and governed by their extensional stiffness (i.e., EA/R).

This paper provides just such guidance. As a starting point, the linear response of circular arches and archlike structures to radial and tangential line loading is examined for both pinned and clamped supports. The point is to model the linear response of solid arches (i.e., without interior hinges) standing on their own and serving as the "foundations" of deck-stiffened arches. Both radially applied and gravitational loading are considered. It will be shown that arch behavior ranges from pure compression to stresses and deflections dominated by elementary beam bending. That behavior change can be explicitly tracked by an arch rise parameter, λ, that is a function of the arch's semivertex angle α, thickness h, and radius R.

The present exposition is concerned with thin arches (i.e., $h/R<1$) and so assumes a linear stress distribution through the thickness and a curvature based on Sanders' shell theory (see Dym 1990) that was developed and used to model the buckling and postbuckling behavior of shallow and steep arches (Schreyer and Masur 1966; Dym 2002).

The paper is organized as follows. The basic arch equations are derived in the next section, "Modeling Arches under General Loading," which also identifies the critical arch parameter. These equations are solved in the section "Arches under Radially Applied Loads." In "Arches under Gravitational Loads," it is shown that the results are the same for cases in which the load is gravitational (i.e., vertical). Key numerical results, limiting cases and displacement and stress resultant approximations are given in "Interpreting Arch Behavior," following which "Conclusions" are then drawn.

Modeling Arches under General Loading

Consider a planar circular arch of constant mean radius R and thickness h, loaded on its outer surface by a radially directed (positive inward) line load q_r and a tangential line load q_θ (Fig. 2). The starting point for a model of the response of the arch to the load is a kinematic model such that the tangential (or circumferential) strain is given by

[1]Fletcher Jones Professor of Engineering Design, Dept. of Engineering, Harvey Mudd College, Claremont, CA 91711 (corresponding author). E-mail: clive_dym@hmc.edu

[2]Emeritus Professor of Engineering, Dept. of Engineering, Harvey Mudd College, Claremont, CA 91711.

Note. This manuscript was submitted on October 14, 2009; approved on June 29, 2010; published online on July 1, 2010. Discussion period open until June 1, 2011; separate discussions must be submitted for individual papers. This paper is part of the ***Journal of Structural Engineering***, Vol. 137, No. 1, January 1, 2011. ©ASCE, ISSN 0733-9445/2011/1-49–58/$25.00.

Fig. 1. Salginatobel Bridge, Schiers, Switzerland (photo reprinted with permission from Madame Marie-Claire Blumer-Maillart)

$$\varepsilon_{\theta\theta}(z,\theta)=\frac{1}{R}\left(\frac{dv(\theta)}{d\theta}-w(\theta)\right)+\frac{z}{R^2}\left(\frac{d^2w(\theta)}{d\theta^2}+\frac{dv(\theta)}{d\theta}\right) \tag{1}$$

where $w(\theta)$ and $v(\theta)$=radial (positive inward) and tangential displacements and z=thickness (positive outward) coordinate.

Eq. (1) is a linear subset of a nonlinear ring equation (Dym 2002) that is itself a one-dimensional subset of the Sanders' (1963) shell equations. (Corresponding results for the Donnell and shallow arch curvatures are discussed below.) The axial and bending stress resultants, $N(\theta)$ and $M(\theta)$, consistent with Eq. (1) are expressed in terms of displacements in the following constitutive relations:

$$N(\theta)=\frac{EA}{R}\left(\frac{dv(\theta)}{d\theta}-w(\theta)\right)$$

$$M(\theta)=-\frac{EI}{R^2}\left(\frac{d^2w(\theta)}{d\theta^2}+\frac{dv(\theta)}{d\theta}\right) \tag{2}$$

where E=Young's modulus and A and I=arch's cross-sectional area and the area's second moment, respectively.

For an arch subject to forces per unit length q_r and q_θ, the first variation of the total potential energy (Dym and Shanes 1973) corresponding to the kinematic result (2) is

$$\delta^{(1)}\Pi=\int_{-\alpha}^{\alpha}\left\{\frac{N}{R}\left[\frac{d\delta v}{d\theta}-\delta w\right]-\frac{M}{R^2}\left(\frac{d^2\delta w}{d\theta^2}+\frac{d\delta v}{d\theta}\right)-q_\theta\delta v-q_r\delta w\right\}Rd\theta \tag{3}$$

where α=arch's semivertex angle (that is, 2α is the arch opening angle). Also, consistent with the various kinematic formulations used herein, it is assumed that the arch is thin so that $(R+z)d\theta \cong Rd\theta$ in Eq. (3). The vanishing of the first variation of the total potential (3) then yields two equations of equilibrium for the loaded arch

$$\frac{1}{R}\frac{dN(\theta)}{d\theta}-\frac{1}{R^2}\frac{dM(\theta)}{d\theta}+q_\theta=0$$

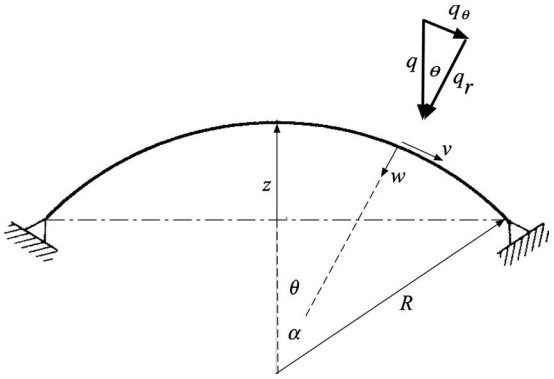

Fig. 2. Geometry of and loading on a thin circular (pinned) arch of radius R and semivertex angle α

$$\frac{N(\theta)}{R}+\frac{1}{R^2}\frac{d^2M(\theta)}{d\theta^2}+q_r=0 \tag{4}$$

Upon the introduction of the transverse shear

$$Q(\theta)=\frac{1}{R}\frac{dM(\theta)}{d\theta} \tag{5}$$

the equations of equilibrium become

$$\frac{dN(\theta)}{d\theta}-Q(\theta)+q_\theta R=0$$

$$N(\theta)+\frac{dQ(\theta)}{d\theta}+q_r R=0 \tag{6}$$

The vanishing of Eq. (3) also produces the following choices of boundary conditions at the ends of the arch, $\theta=\pm\alpha$:

$$\text{Either } N(\pm\alpha)-\frac{M(\pm\alpha)}{R}=0 \text{ or } \delta v(\pm\alpha)=0 \tag{7a}$$

$$\text{Either } Q(\pm\alpha)=\frac{1}{R}\frac{dM(\pm\alpha)}{d\theta}=0 \text{ or } \delta w(\pm\alpha)=0 \tag{7b}$$

$$\text{Either } M(\pm\alpha)=0 \text{ or } \delta\left(\frac{dw(\pm\alpha)}{d\theta}\right)=0 \tag{7c}$$

It is worth noting one more point about the nature of the solutions being sought. The equations derived above are valid for any relatively thin arch (or ring) for which $h/R \ll 1$, but for any value of the circumferential angle θ. However, it will prove useful to make an additional modeling assumption, namely, that all angles θ are sufficiently small that $\sin\theta \cong \theta$ and $\cos\theta \cong 1$ or $\cos\theta \cong 1-\theta^2/2$, depending on the context. Note that this "small angle" approximation is good even for relatively large angles: for $\alpha=45^\circ \cong 0.79$ rad, $\sin(0.79)=\cos(0.79) \cong 0.71$ and $1-(0.71)^2/2 \cong 0.69$. Thus, the small angle approximation can include arches whose total opening angles are as large as $2\alpha=90^\circ \cong 1.572$ rad. The physical import of the small angle assumption is that the arch rise f (see Fig. 2) can be written and then approximated as

$$\frac{f}{R}=(1-\cos\alpha) \cong \frac{\alpha^2}{2} \tag{8}$$

Thus, the assumption of small angles implies a concomitant assumption that the arch has a small rise and may be considered a shallow arch.

Arches under Radially Applied Loading

Assuming that the arch responds symmetrically to a (symmetric) uniform line load $q_r=q$ with $q_\theta=0$, the stress resultants can be found by integrating Eqs. (5) and (6)

$$N(\theta) = -qR(1 + C_1 \cos\theta)$$

$$M(\theta) = qR^2(C_2 - C_1 \cos\theta)$$

$$Q(\theta) = qR(C_1 \sin\theta) \tag{9}$$

The constants C_i are determined by satisfying boundary conditions. Equations for the displacements v and w are then found by substituting the stress resultants (9) into the constitutive Eq. (2). After some straightforward manipulation, the governing equations for the displacements are found to take the following forms:

$$\frac{dv(\theta)}{d\theta} - w(\theta) = -\frac{qR^2}{EA}(1 + C_1 \cos\theta)$$

$$\frac{d^2w(\theta)}{d\theta^2} + \frac{dv(\theta)}{d\theta} = -\left(\frac{qR^2}{EA}\right)\left(\frac{1}{\bar{I}}\right)(C_1 \cos\theta - C_2) \tag{10}$$

Note the introduction in Eq. (10) of a dimensionless ratio $\bar{I} = I/AR^2$, which for rectangular cross sections ($A=bh, I=bh^3/12$) means that $\bar{I}=h^2/12R^2$. Eq. (10) are readily uncoupled and integrated to find the following solutions: the (inwardly positive) radial displacement is symmetric about $\theta=0$:

$$w(\theta) = \frac{qR^4}{EI}\left\{\left[\left(\frac{1+\bar{I}}{2}\right)\theta \sin\theta\right]C_1 - C_2 + (\bar{I}\cos\theta)C_3 + \bar{I}\right\} \tag{11}$$

and the tangential displacement is antisymmetric about $\theta=0$

$$v(\theta) = \frac{qR^4}{EI}\left\{[(1-\bar{I})\sin\theta - (1+\bar{I})\theta\cos\theta]\frac{C_1}{2} - (\bar{I}\theta)C_2 + (\bar{I}\sin\theta)C_3\right\} \tag{12}$$

The three unknown constants in the solutions (9), (11), and (12) can now be determined for any arch, subject to appropriate boundary conditions. For a simply supported arch, those boundary conditions are

$$w(\pm\alpha) = 0, \quad v(\pm\alpha) = 0, \quad M(\pm\alpha) = 0 \tag{13}$$

The resulting solution for small angles α (see Appendix I for details) is expressed in terms of a dimensionless factor $2\alpha^4/15\bar{I}$ in which α and $\bar{I}$ are not independent. In fact, the factor $2\alpha^4/15\bar{I}$ is a variant of an arch rise parameter introduced in an exploration of the postbuckling behavior of shallow arches by Schreyer and Masur (1966). They defined a dimensionless *arch rise parameter* λ as the ratio of the arch rise f to one-half of the arch thickness h

$$\lambda = \frac{f}{h/2} = \frac{2R}{h}(1 - \cos\alpha) \cong \alpha^2\frac{R}{h} \tag{14a}$$

Given the definitions of $\bar{I}$ and λ, it also follows that

$$\lambda^2 \equiv \alpha^4/(12\bar{I}) \tag{14b}$$

For shallow arches, the general solutions (9), (11), and (12) are simplified by expanding the trigonometric terms in the solutions to account both for small semivertex angles α and for correspondingly small values of the circumferential coordinate θ, since $-\alpha \leqslant \theta \leqslant \alpha$. (Numerical values and limiting cases are presented below in the section entitled "Interpreting Arch Behavior.") For pinned arches, with particular attention to orders of magnitude, it turns out that the (inward) radial deflection at the crown of the arch ($\theta=0$) is

$$w^p(0) \cong \frac{5\lambda^2/2}{1 + 8\lambda^2/5}\left(\frac{qR^2}{EA}\right) \equiv \frac{1}{1 + 8\lambda^2/5}\left(\frac{5qL^4}{384EI}\right) \tag{15}$$

where it has been noted that the developed length of a shallow arch is essentially equal to its span length, $L=2R\sin\alpha \cong 2R\alpha = S$. The axial stress resultant behaves as

$$N^p(\theta) \cong -qR\left(\frac{8\lambda^2/5}{1 + 8\lambda^2/5}\right) \tag{16}$$

Similarly, the moment resultant is

$$M^p(\theta) \cong \frac{qL^2/8}{1 + 8\lambda^2/5}(1 - (\theta/\alpha)^2) \tag{17}$$

The transverse shear is

$$Q^p(\theta) \cong -\frac{qL/2}{1 + 8\lambda^2/5}(\theta/\alpha) \tag{18}$$

The circumferential stress can be calculated using the one-dimensional version of Hooke's Law, $\sigma_{\theta\theta}(z,\theta)=E\varepsilon_{\theta\theta}(z,\theta)$, along with Eqs. (1) and (2)

$$\sigma_{\theta\theta}(z,\theta) = \frac{N(\theta)}{A} - \frac{M(\theta)z}{I} \tag{19}$$

The stress at the crown of the pinned arch is found by substituting the in-plane (16) and bending (17) resultants in their simple limit forms, into Eq. (19), where a rectangular cross section is again assumed

$$\sigma^p_{\text{crown}} = \sigma^p_{\theta\theta}(z, \theta = 0) = -\frac{qR/A}{1 + 8\lambda^2/5}\left[\overbrace{8\lambda^2/5}^{\text{compression}} + \left(\frac{2z}{h}\right)\overbrace{3\lambda}^{\text{bending}}\right] \tag{20}$$

The last result to be determined for the pinned arch is the set of inwardly directed horizontal and upwardly directed vertical reaction forces. For the continuing small angle assumption, and with the moment at the supports ($\theta = \mp\alpha$) self-evidently trivial

$$R^p_H = qR\left(\frac{(8\lambda^2/5)}{1 + 8\lambda^2/5}\right) \text{ and } R^p_V = qR\alpha = \frac{qL}{2} \tag{21}$$

Note that the arguments of all the results given in Eqs. (15)–(18), (20), and (21) for the pinned arch depend explicitly only on the arch rise parameter λ.

Eqs. (15)–(18), (20), and (21) suggest that for small angles α, arch behavior depends explicitly on the arch rise parameter λ, and that λ will be influential in delineating different regimes of arch

Table 1. Crown Displacements, Stress Resultants, Stresses, and Reactions for Small Values of Opening Arch Angle α

	Pinned arches	Clamped arches
Crown displacement	$w^p(0) \cong \frac{5\lambda^2/2}{1+8\lambda^2/5}\left(\frac{qR^2}{EA}\right)$	$w^c(0) \cong \frac{\lambda^2/2}{1+4\lambda^2/15}\left(\frac{qR^2}{EA}\right)$
Axial resultant	$N^p(\theta) = -qR\left(\frac{8\lambda^2/5}{1+8\lambda^2/5}\right)$	$N^c(\theta) = -qR\left(\frac{4\lambda^2/15}{1+4\lambda^2/15}\right)$
Moment resultant	$M^p(\theta) = \frac{qL^2/8}{1+8\lambda^2/5}\left(1-\left(\frac{\theta}{\alpha}\right)^2\right)$	$M^c(\theta) = \frac{qL^2/24}{1+4\lambda^2/15}\left(1-3\left(\frac{\theta}{\alpha}\right)^2\right)$
Shear resultant	$Q^p(\theta) = -\frac{qL/2}{1+8\lambda^2/5}\left(\frac{\theta}{\alpha}\right)$	$Q^c(\theta) = -\frac{qL/2}{1+4\lambda^2/15}\left(\frac{\theta}{\alpha}\right)$
Axial stress (pinned)	$\sigma^p_{\text{crown}} = \sigma^p_{\theta\theta}(z,\theta=0) = -\frac{qR/A}{1+8\lambda^2/5}\left[\overbrace{8\lambda^2/5}^{\text{compression}} + \left(\frac{2z}{h}\right)\overbrace{3\lambda}^{\text{bending}}\right]$	
Axial stress (clamped)	$\sigma^c_{\text{crown}} = \sigma^c_{\theta\theta}(z,\theta=0) = -\frac{qR/A}{1+4\lambda^2/15}\left[\overbrace{4\lambda^2/15}^{\text{compression}} + \left(\frac{2z}{h}\right)\overbrace{\lambda}^{\text{bending}}\right]$	
Horizontal reactions	$R^p_H = qR\left(\frac{8\lambda^2/5}{1+8\lambda^2/5}\right)$	$R^c_H = qR\left(\frac{4\lambda^2/15}{1+4\lambda^2/15}\right)$
Vertical reactions	$R^p_V = qL/2$	$R^c_V = qL/2$
Support moments	$M^p(\pm\alpha) = 0$	$M^c(\pm\alpha) = \mp\frac{qL^2/12}{1+4\lambda^2/15}$

behavior. In particular, it will be seen that for small values of λ ($\lambda \ll 1$), the arch in fact flattens completely and behaves like a beam in bending; for large values of λ ($\lambda \gg 1$), the arch behaves as a true arch with a uniformly compressive state of stress. In each of the foregoing inequalities, 1 has been used as the standard or unit of measurement. In fact, it will be shown that the standard varies with the boundary conditions: for pinned arches the standard reflects how $8\lambda^2/5$ compares with 1, while for clamped arches the standard reflects how $4\lambda^2/15$ compares to 1. It is interesting that these two standards appear as factors in the corresponding buckling loads of pinned and clamped arches (Dym 2002). (It is also interesting to observe that these same two factors emerge when the Donnell and shallow arch curvatures are employed below to formulate the same problems.)

When the arch is clamped at its boundaries, the appropriate boundary conditions are

$$w^c(\pm\alpha) = 0, \quad v^c(\pm\alpha) = 0, \quad \frac{dw^c(\pm\alpha)}{d\alpha} = 0 \tag{22}$$

The unknown constants in the solutions (9), (11), and (12) are now determined for the clamped arch, and the following results are found (again, see Appendix I for details). For fixed arches for which $\alpha^2 \ll 1$, the (inward) radial deflection at the crown of the arch ($\theta = 0$) is

$$w^c(0) \cong \frac{\lambda^2/2}{1+4\lambda^2/15}\left(\frac{qR^2}{EA}\right) \equiv \frac{1}{1+4\lambda^2/15}\left(\frac{qL^4}{384EI}\right) \tag{23}$$

The axial stress result is

$$N^c(\theta) \cong -qR\left(\frac{4\lambda^2/15}{1+4\lambda^2/15}\right) \tag{24}$$

Similarly, the moment resultant is

$$M^c(\theta) \cong \frac{qL^2/24}{1+4\lambda^2/15}(1-3(\theta/\alpha)^2) \tag{25}$$

Also similarly, the shear resultant is

$$Q^c(\theta) \cong -\frac{qL/2}{1+4\lambda^2/15}\left(\frac{\theta}{\alpha}\right) \tag{26}$$

The stress at the crown of the clamped arch is again found by substituting the appropriate stress resultants $N(\theta)$ and $M(\theta)$ into Eq. (19), where the usual rectangular cross section is assumed

$$\sigma^c_{\text{crown}} = \sigma^c_{\theta\theta}(z,\theta=0) = -\frac{qR/A}{1+4\lambda^2/15}\left[\overbrace{4\lambda^2/15}^{\text{compression}} + \left(\frac{2z}{h}\right)\overbrace{\lambda}^{\text{bending}}\right] \tag{27}$$

The final results to be determined for the clamped arch are the (inward) horizontal and (upward) vertical reaction forces and the support moment. For small angles

$$R_H^c = qR\left(\frac{4\lambda^2/15}{1+4\lambda^2/15}\right), \quad R_V^c = qR\alpha = \frac{qL}{2}$$

$$M^c(\pm\alpha) = -\frac{qL^2/12}{1+4\lambda^2/15} \tag{28}$$

For the clamped arch, as with the pinned arch, the arguments of all the results given in Eqs. (23)–(28) functionally depend only on the arch rise parameter λ, as can be seen in the results shown in Table 1.

While the results are not presented here, the particulars of a Donnell-type solution appear *exactly* like those obtained in the foregoing Sanders-based analysis, with *no* noticeable difference in the end results. In other words, *all* of the other results presented (i.e., the circumferential stress $N(\theta)$, moment $M(\theta)$, shear $Q(\theta)$, and the deflection $w(0)$ at the crown) are exactly the same as those given above for both the small angle approximation and for the limiting λ cases. The only distinction between a Donnell-based solution and its Sanders-based counterparts is that it becomes more obvious that the axial resultant $N_D(\theta)$ is a constant when the tangential load q_θ is absent.

When shallow arch theory is used to model this problem, the analysis is much easier than for the Sanders and Donnell analyses. Some details are displayed in Appendix II, wherein their elegant simplicity can be observed, including the fact that the arch deflected shapes clearly match the deflection patterns of corresponding flat beams. And, once again, the basic formulas and the numerical results for shallow arch theory are indistinguishable from those of their Sanders and Donnell counterparts.

Arches under Gravitational Loading

For the case of gravitational loading, for which $q_r = \rho g A \cos\theta$ and $q_\theta = \rho g A \sin\theta$, the solutions for any of the three arch theories (Sanders, Donnell, and shallow) appear much as the foregoing, albeit with significantly more algebra. With the Sanders curvature formulation the governing equilibrium equations are, with $q = \rho g A$

$$\frac{1}{R}\frac{dN(\theta)}{d\theta} - \frac{1}{R^2}\frac{dM(\theta)}{d\theta} + q\sin\theta = 0$$

$$\frac{N(\theta)}{R} + \frac{1}{R^2}\frac{d^2M(\theta)}{d\theta^2} + q\cos\theta = 0 \tag{29}$$

In this case the general solutions for the stress resultants are

$$N(\theta) = qR(C_1\cos\theta - \theta\sin\theta)$$

$$M(\theta) = qR^2[C_1\cos\theta + C_2 - (\cos\theta + \theta\sin\theta)] \tag{30}$$

and the radial deflection is

$$w(\theta) = \frac{qR^4}{4EI}[-(2(1+\bar{I})\theta\sin\theta)C_1 - 4C_2 + C_3\cos\theta + (3+\bar{I})\theta\sin\theta - (1+\bar{I})\theta^2\cos\theta] \tag{31}$$

The algebra involved for a Sanders-based analysis of a gravity-loaded arch is considerably longer and messier than for the radial loading, hence only numerical resultants are presented in Tables 2 and 3. Therein are displayed values of the stress resultants and the radial displacement alongside the exact and approximate results for the arches under radial loading, and it can be seen that they differ by no more than a few percent. That is, the circumferential and bending stress resultants and the radial displacement at the arch crown under gravitational loading are virtually identical to those under radially directed loading when α is small (e.g., $\alpha = 0.20$). The moment resultant values differ modestly when the arch opening angle and the arch rise parameter are large (i.e., $\alpha = 0.80$, $\lambda \geq 4$).

Table 2. Exact and Approximate (Small α) Axial and Moment Stress Resultants and Radial Displacements at the Crown of Pinned Arches under Radially Directed and Gravity ($q = \rho g A$) Loads

	$-N(0)/qR$				
	Exact (central)			Exact (gravity)	
λ	α=0.20	α=0.80	Approx.	α=0.20	α=0.80
1	0.6142	0.5974	0.6154	0.6069	0.4832
2	0.8646	0.8615	0.8649	0.8571	0.7410
4	0.9624	0.9618	0.9624	0.9548	0.8389
8	0.9903	0.9902	0.9903	0.9827	0.8666
10	0.9938	0.9937	0.9938	0.9862	0.8700
	$10^2(M(0)/qL^2)$				
	Exact (radial)			Exact (gravity)	
λ	α=0.20	α=0.80	Approx.	α=0.20	α=0.80
1	4.807	4.769	4.808	4.814	4.845
2	1.686	1.641	1.689	1.697	1.791
4	0.4689	0.4530	0.4699	0.4803	0.6315
8	0.1206	0.1163	0.1209	0.1324	0.3028
10	0.0774	0.0746	0.0781	0.0893	0.2622
	$10^2(EIw(0)/qL^4)$				
	Exact (radial)			Exact (gravity)	
λ	α=0.20	α=0.80	Approx.	α=0.20	α=0.80
1	0.5022	0.5265	0.5008	0.5020	0.5266
2	0.1762	0.1802	0.1760	0.1762	0.1816
4	0.0490	0.0497	0.0490	0.0491	0.0523
8	0.0126	0.0127	0.0126	0.0128	0.0158
10	0.0081	0.0082	0.0081	0.0083	0.0114

The shallow arch equilibrium equations under gravitational loading are

$$\frac{dN_s(\theta)}{d\theta} + \rho g A R\sin\theta = 0$$

$$N_s(\theta) + \frac{1}{R}\frac{d^2M_s(\theta)}{d\theta^2} + \rho g A R\cos\theta = 0 \tag{32}$$

The solutions to Eq. (32) are straightforwardly found as

$$N_s(\theta) = C_1 + \rho g A R\cos\theta$$

$$M_s(\theta) = -\frac{C_1 R}{2}\theta^2 + C_2 + 2\rho g A R^2\cos\theta \tag{33}$$

The solutions (33) differ from their corresponding results (30) for radially directed loading only by the appearance of two trigono-

Table 3. Exact and Approximate (Small α) Axial and Moment Stress Resultants and Radial Displacements at the Crown of Clamped Arches under Radially Directed and Gravity ($q=\rho gA$) Loads

	$-N(0)/qR$				
	Exact (central)			Exact (gravity)	
λ	α=0.20	α=0.80	Approx.	α=0.20	α=0.80
1	0.2065	0.1506	0.2105	0.2001	0.0544
2	0.5148	0.4978	0.5161	0.5086	0.4033
4	0.8100	0.8094	0.8101	0.8041	0.7165
8	0.9447	0.9453	0.9446	0.9389	0.8530
10	0.9639	0.9643	0.9639	0.9581	0.8722

	$10^2(M(0)/qL^2)$				
	Exact (radial)			Exact (gravity)	
λ	α=0.20	α=0.80	Approx.	α=0.20	α=0.80
1	3.299	3.428	3.292	3.310	3.557
2	2.018	2.026	2.018	2.026	2.149
4	0.7899	0.7690	0.7918	0.7978	0.8853
8	0.2300	0.2209	0.2308	0.2374	0.3345
10	0.1502	0.1439	0.1507	0.1575	0.2572

	$10^2(EIw(0)/qL^4)$				
	Exact (radial)			Exact (gravity)	
λ	α=0.20	α=0.80	Approx.	α=0.20	α=0.80
1	0.2069	0.2342	0.2053	0.2072	0.2461
2	0.1265	0.1350	0.1258	0.1267	0.1396
4	0.0495	0.0509	0.0494	0.0497	0.0533
8	0.0144	0.0146	0.0144	0.0145	0.0164
10	0.0094	0.0095	0.0094	0.0095	0.0112

metric terms in place of simple powers of the arch variable θ. Similarly, the deflection is

$$w_s(\theta) = \frac{C_1 R^3}{24EI}\theta^4 - \frac{C_2 R^2}{2EI}\theta^2 + C_3 + \frac{2\rho gAR^4}{EI}\cos\theta \tag{34}$$

Not surprisingly, the results for such gravitational loading on arches with small vertex angles α are essentially identical to those for the radially loaded arch. Thus, only some highlights are given here. For example, for a pinned shallow arch model, the axial stress resultant is

$$N_s^p(\theta) \cong -\rho gAR\left(\frac{1+16\lambda^2/5}{1+8\lambda^2/5} - \cos\theta\right) \cong -\frac{8\lambda^2/5}{1+8\lambda^2/5}\rho gAR \tag{35}$$

the moment resultant is

$$M_s^p(\theta) \cong \rho gAR^2\left[2(\cos\theta - \cos\alpha) - \frac{1+16\lambda^2/5}{2(1+8\lambda^2/5)}(\theta^2-\alpha^2)\right]$$
$$\cong \frac{\rho gA(\alpha R)^2}{2(1+8\lambda^2/5)}\left(1-\left(\frac{\theta}{\alpha}\right)^2\right) = \frac{\rho gAL^2/8}{1+8\lambda^2/5}\left(1-\left(\frac{\theta}{\alpha}\right)^2\right) \tag{36}$$

and the corresponding deflection at the crown of the pinned shallow arch is

$$w_s^p(0) \cong \frac{5\lambda^2/2}{1+8\lambda^2/5}\left(\frac{\rho gAR^2}{EA}\right) \equiv \frac{1}{1+8\lambda^2/5}\left(\frac{5\rho gAL^4}{384EI}\right) \tag{37}$$

Since $q=\rho gA$ here, it is evident that these results correspond exactly to those obtained for radially direction loading [see Eqs. (53), (54), and (56), respectively].

Interpreting Arch Behavior

The principal results derived in the section "Arches under Radially Applied Loading" appear in Eqs. (15)–(18), (20), and (21) for pinned arches, and Eqs. (23)–(28) for clamped arches; they are also summarized in Table 1. These analytical results, obtained under the small angle assumption, comprise a useful set of closed form estimates of the behaviors of the radial displacement at the crown; the axial, moment and shear stress resultants; the stress at the crown; and the reactions at the arch supports. These displacement and stress estimates are explicit functions of the arch rise parameter λ, but not of the semivertex angle α.

Now, despite the small angle assumption, these results were also quite similar for comparatively large values of α. As can be seen first in Table 2, which compares exact results for pinned arches from the Sanders formulation to its small angle approximation, the axial and moment resultants and the radial or transverse displacement are virtually identical for α=0.20 and α=0.80. Table 3 shows results almost as good for clamped arches, with a 33% difference in the axial resultant and a 15% difference in the radial displacement when λ=1. The data in Tables 2 and 3 also show consistent variations in the various physical quantities as the value of the arch rise parameter λ changes, but they do not change very much with the opening angle α. The data in Tables 2 and 3 thus confirm that the estimates of the major variables of interest given in Table 1 can be regarded as solid and widely applicable over broad, practical ranges of λ.

Tables 4 and 5 display several limiting cases that are derived from the analytical estimates of Table 1. It is evident in Table 4 that for arches with very small rises, for which $\lambda^2 \ll 1$, all of the quantities involved (i.e., the radial displacement, all three stress resultants, the axial stress, and the support reactions) tend to the results that would be expected for classic beam behavior. That is, as λ^2 becomes very small, an extremely shallow arch behaves exactly like a beam under a uniform line load q, even to the classic Mc/I form of the compressive stress at the arch crown.

Conversely, as can be seen in Table 5, as λ^2 becomes very large, an arch behaves much as one would expect an arch or a ring segment of width b to respond when loaded by a pressure $p=q/b$ because then $qR/EA=(q/b)R/Eh$. In particular, the stress is uniformly compressive through the thickness, and the influence (or presence) of the moment, shear and transverse boundary conditions are inconsequential. Furthermore, the crown radial displacement takes on a form remarkably similar to that seen in thin rings and shells when the rise parameter takes on large values ($\lambda^2 \gg 1$), although it is interesting to note that the centerline deflection of the clamped arch is *larger* than the corresponding deflection of the pinned arch, suggesting that for $\lambda^2 \gg 1$ a pinned arch is stiffer than a clamped arch. In fact, one measure of the stiffness of the loaded arch is the ratio of the pinned to the clamped crown displacement. That stiffness measure, derived from Eqs. (15) and (23), respectively, is

Table 4. Limiting Values of Crown Displacements, Stress Resultants, Stresses, and Reactions for Large Rises, i.e., Small Values of the Arch Rise Parameter λ

	Pinned arches ($8\lambda^2/5 \ll 1$)	Clamped arches ($4\lambda^2/15 \ll 1$)
Radial displacement ($\theta=0$)	$w^p(0) \cong \frac{5qL^4}{384EI}$	$w^c(0) \cong \frac{qL^4}{384EI}$
Axial resultant	$N^p(\theta) \cong 0$	$N^c(\theta) \cong 0$
Moment resultant ($\theta=0$)	$M^p(\theta) \cong \frac{qL^2}{8}\left(1-\left(\frac{\theta}{\alpha}\right)^2\right)$	$M^c(\theta) \cong \frac{qL^2}{24}\left(1-3\left(\frac{\theta}{\alpha}\right)^2\right)$
Shear resultant ($\theta=0$)	$Q^p(\theta) \cong -\frac{qL}{2}\left(\frac{\theta}{\alpha}\right)$	$Q^c(\theta) \cong -\frac{qL}{2}\left(\frac{\theta}{\alpha}\right)$
Axial stress ($z=h/2,\ \theta=0$)	$\sigma^p_{\text{crown}} \cong \underbrace{-\left(\frac{qL^2}{8}\right)\left(\frac{h}{2}\right)\left(\frac{12}{bh^3}\right)}_{Mc/I}$	$\sigma^c_{\text{crown}} \cong \underbrace{-\left(\frac{qL^2}{24}\right)\left(\frac{h}{2}\right)\left(\frac{12}{bh^3}\right)}_{Mc/I}$
Horizontal reactions	$R^p_H = qR(8\lambda^2/5) \Rightarrow 0$	$R^c_H = qR(4\lambda^2/15) \Rightarrow 0$
Vertical reactions	$R^p_V = \frac{qL}{2}$	$R^c_V = \frac{qL}{2}$
Support moments	$M^p(\pm\alpha)=0$	$M^c(\pm\alpha) = \mp\frac{qL^2}{12}$

$$k_{\text{arch}} \sim \frac{w^p(0)}{w^c(0)} = 5\left(\frac{1+4\lambda^2/15}{1+8\lambda^2/5}\right) \tag{38}$$

Eq. (38) shows that for very small values of λ, the crown deflection of the pinned arch/beam will be larger than for its clamped counterpart, indicating that the clamped arch beam is stiffer that the pinned beam, an unsurprising result. On the other hand, as λ gets very large, the ratio in Eq. (38) decreases, goes through the value 1 when $\lambda_{p=c}=\sqrt{15}\cong 3.873$, and then stabilizes in an asymptote

$$k^{\text{asymp}}_{\text{arch}}|_{\lambda^2 \gg 1} = \frac{5}{6} \tag{39}$$

In addition to providing the correct (and thus reassuring) limiting cases, the estimates displayed in Table 1 also provide a means for identifying the transition from the bending behavior of curved beams to that of essentially uniform compression of "pure" arches. Clearly that transition occurs as $8\lambda^2/5 \gg 1$ for pinned arches and as $4\lambda^2/15 \gg 1$ for clamped arches. There are several different judgments that are possible about just when that

Table 5. Limiting Values of Crown Displacements, Stress Resultants, Stresses, and Reactions for Large Rises, i.e., Large Values of the Arch Rise Parameter λ

	Pinned arches ($8\lambda^2/5 \gg 1$)	Clamped arches ($4\lambda^2/15 \gg 1$)
Radial displacement ($\theta=0$)	$w^p(0) = \left(\frac{25}{16}\right)\frac{qR^2}{EA}$	$w^c(0) = \left(\frac{15}{8}\right)\frac{qR^2}{EA}$
Axial resultant	$N^p(\theta) \cong -qR$	$N^c(\theta) \cong -qR$
Moment resultant ($\theta=0$)	$M^p(\theta) \cong 0$	$M^c(\theta) \cong 0$
Shear resultant ($\theta=0$)	$Q^p(\theta) \cong 0$	$Q^c(\theta) \cong 0$
Axial stress ($z=h/2,\ \theta=0$)	$\sigma^p_{\text{crown}} \cong -\frac{qR}{A}$	$\sigma^c_{\text{crown}} \cong -\frac{qR}{A}$
Horizontal reactions	$R^p_H = qR$	$R^c_H = qR$
Vertical reactions	$R^p_V = qL/2$	$R^c_V = qL/2$
Support moments	$M^p(\pm\alpha)=0$	$M^c(\pm\alpha) = -\frac{5qL^2}{16\lambda^2} \Rightarrow 0$

Table 6. Values of Various Measured [Span, Rise, Thickness (Billington 1979)] and Calculated (Radius, Semivertex Angle, Rise) Arch Parameters for the Underlying Arches of Robert Maillart's Deck-Stiffened Arches

Bridge	L	f	h	R	h/R	α	λ
Flienglibach	38.7	5.17	0.25	38.8	0.0064	0.52	42.2
Schrähbach	28.8	4.02	0.18	27.8	0.0065	0.54	45.8
Valtschielbach	43.2	5.20	0.23	47.5	0.0048	0.47	46.1
Landquart	30.0	7.90	0.26	18.2	0.0143	0.97	65.8
Spital	30.0	3.26	0.24	36.1	0.0066	0.43	27.6
Landholz	26.0	3.40	0.16	26.6	0.0060	0.51	43.4
Hombach	21.0	3.00	0.16	19.9	0.0080	0.56	38.5
Luterstalden	12.5	2.55	0.16	8.9	0.0180	0.77	33.5
Traubach	40.0	5.60	0.20	38.5	0.0052	0.55	57.4
Bohlbach	14.4	2.70	0.16	11.0	0.0145	0.72	35.2
Schwandbach	37.4	6.00	0.20	32.1	0.0062	0.62	62.0
Töll	38.0	3.50	0.14	53.3	0.0026	0.36	50.6

transition occurs. For example, in parallel with the classic notion of an arch constituted of a set of masonry blocks that cannot sustain a tensile stress (Heyman 1995), the transition to arch behavior could be defined as occurring at that value of λ which ensures that the axial stress is in compression through the arch thickness. Thus, applying that condition to Eq. (20) for pinned arches produces the transition point of

$$3\lambda^p_{\text{trans}} \leqslant 8(\lambda^p_{\text{trans}})^2/5 \Rightarrow \lambda^p_{\text{trans}} = (\alpha^2 R/h)_{\text{trans}} \geqslant 1.88 \qquad (40)$$

Similarly, from Eq. (27) for clamped arches the transition occurs at

$$\lambda^c_{\text{trans}} \leqslant 4(\lambda^c_{\text{trans}})^2/15 \Rightarrow \lambda^c_{\text{trans}} = (\alpha^2 R/h)_{\text{trans}} \geqslant 3.75 \qquad (41)$$

This is somewhat more restrictive than, but similar to, another suggested criterion in which the resultant compressive force is within the arch cross section (Heyman 1995).

Another transition estimator could be based on the idea that the dimensionless axial stress resultant might attain a preassigned fraction of a pure membrane state; for example, $|N(\theta)/qR| \cong 0.90$, that is, the axial stress resultant would be 90% of that membrane state. In this case, the corresponding estimates of behavioral transition points are

$$8(\lambda^p_{\text{trans}})^2/5 \cong 9 \Rightarrow \lambda^p_{\text{trans}} = (\alpha^2 R/h)_{\text{trans}} \cong 2.37 \qquad (42)$$

for pinned arches and

$$4(\lambda^c_{\text{trans}})^2/15 \cong 9 \Rightarrow \lambda^c_{\text{trans}} = (\alpha^2 R/h)_{\text{trans}} \cong 5.81 \qquad (43)$$

for clamped arches. Thus, for clamped arches, the transition to an almost pure compressive state will occur for those arches with significantly larger rises.

Perhaps the most interesting results, especially in historical terms, are those displayed in Table 6, which lists measured and calculated arch parameters for a dozen of Robert Maillart's deck-stiffened arch bridges. It is quite clear that the rise parameter λ calculated for each of these bridges is a very large number. In fact, and especially in the light of the immediately foregoing discussion, there can be no doubt that the basic arches in Maillart's designs were very much in the uniform compressive state that he intended. It is also worth noting that the large values of λ also confirm another of Maillart's intuitions, namely, that the requisite membrane state could be developed and sustained in relatively thin arches, which are esthetically more pleasing and suggestive of the force developed within them.

As noted above, Maillart analyzed his designs in a far simpler and more direct manner, and his intuitions were more than adequately confirmed. Interestingly enough in Switzerland at that time, all designs were confirmed experimentally, not theoretically, as that was felt to be the most provident path to take for design in a public environment (Billington 1979), both from the standpoint of the governing public authorities and of the leading engineers of the time who understood that their understanding of the issues was not yet established beyond question. Still further, and in this context rather ironically, Maillart believed (Billington 1979) "in the priority of design over analysis, in the subordinate role of analysis as a tool of design." In fact, in Maillart's own words, "Only a fully simplified method of analysis is…both possible and sufficient." Of course, it might be counter-argued that Maillart's modeling ideas were confirmed only because his designs were very conservative in the sense that their values of λ were very large!

Conclusions

This paper explored the linear response of circular arch structures to radially directed, "dead" pressure loading and to gravitational loading. It was shown that arch behavior ranges from elementary beam bending for very shallow arch structures, to a pure compressive state for steep arches. The change in response can be tracked with an arch rise parameter that is a function of the arch's semivertex angle, thickness, and radius: $\lambda = \alpha^2 R/h$. The transition from beam to arch behavior occurs for $\lambda^p_{\text{trans}} \sim 2$ for pinned arches and for $\lambda^c_{\text{trans}} \sim 4$ for clamped arches. The "theory" also showed that Robert Maillart's inspired design concept performed exactly as he intended in that the compressive states he posited were clearly and completely created in elegant slender arches.

Simple closed-form estimates, useful for back-of-the-envelope analysis and design calculations, were presented for the major displacements and stress resultants. It was also noted that virtually identical results are obtained when three different curvature expressions (e.g., Sanders, Donnell, and shallow) are used, with the distinctions between the results being quite small, for small values of α. This suggests that (1) the far simpler shallow arch theory can be safely used and (2) that differences in arch behavior are far more sensitive to the formulation of the midsurface strain than to changes in the curvature expression. Thus, the estimates presented for the important displacement and stress resultants can be applied with confidence to such arch structures over wide ranges of the arch opening angle and the arch rise parameter. Finally, these design-and-analysis estimates were shown to be as

valid for gravitational loading as they are for radially directed loads for small values of the arch opening angle, that is, for shallow arches.

Acknowledgments

The writers appreciate interesting conversations with Nikolas Sherrow-Groves, HMC '08, that helped stimulate this line of inquiry, and they are also grateful for several thoughtful and constructive reviews.

Appendix I. Radially Loaded Arch Solution Details

The details encompassing the solutions (9) and (10) are as follows. For the pinned arch, with the boundary conditions (13), three equations are found for the three constants, and they can be solved to yield

$$C_{1p} = -\frac{2\bar{I}\sin\alpha}{D_p}$$

$$C_{2p} = -\frac{\bar{I}\sin 2\alpha}{D_p}$$

$$C_{3p} = \frac{(\sin\alpha - 3\alpha\cos\alpha) - \bar{I}(\sin\alpha + \alpha\cos\alpha)}{D_p} \tag{44}$$

where the common denominator D_p is

$$D_p = (2\alpha + \alpha\cos 2\alpha - (3/2)\sin 2\alpha) + \bar{I}(\alpha + \sin 2\alpha/2) \tag{45}$$

When Eq. (45) is approximated for small angles α, it is found that

$$D_p \cong 2\alpha\bar{I}[1 + 2\alpha^4/(15\bar{I})] \tag{46}$$

Given that both α and $\bar{I}$ are small numbers, the evaluation of the dimensionless factor $2\alpha^4/15\bar{I}$ in Eq. (46) needs attention. The structure of Eq. (46) suggests that α and $\bar{I}$ are not independent, and that the dimensionless factor $2\alpha^4/15\bar{I}$ is the parameter that needs to be considered. In fact, the factor $2\alpha^4/15\bar{I}$ can be written in terms the arch rise parameter introduced by Schreyer and Masur (1966) and noted above as Eq. (14*a*). In terms of Eq. (14) then, Eq. (46) can be recast as:

$$D_p \cong 2\alpha\bar{I}(1 + 8\lambda^2/5) \tag{47}$$

While corresponding approximations for the constants C_{ip} [Eq. (44)] are then possible, it is important to keep in mind that these constants are rarely evaluated in isolation. For example, the moment resultant at the crown ($\theta=0$) of a pinned arch is found from Eq. (9) as

$$M(0) = qR^2(C_{2p} - C_{1p}) = qR^2\frac{\bar{I}(2\sin\alpha - \sin 2\alpha)}{D_p}$$

$$\cong qR^2\frac{\bar{I}(2\alpha - \alpha^3/3 - 2\alpha + 4\alpha^3/3)}{D_p} = \frac{qR^2\bar{I}\alpha^3}{D_p} \tag{48}$$

so that higher-order terms in α^n (sometimes to $n=5$ or 6) must be kept in order to avoid truncation errors. Expressed in terms of the arch's span length, Eq. (48) is

$$M(0) \cong \frac{q(R\alpha)^2\bar{I}\alpha}{2\alpha\bar{I}(1 + 8\lambda^2/5)} = \frac{qL^2/8}{(1 + 8\lambda^2/5)} \tag{49}$$

For a clamped arch, satisfying boundary conditions (22), the three constants are

$$C_{1c} = -\frac{2\bar{I}\alpha\sin\alpha}{D_c}$$

$$C_{2c} = -\frac{2\bar{I}\sin^2\alpha}{D_c}$$

$$C_{3c} = -\frac{(1 + \bar{I})(\alpha\sin\alpha + \alpha^2\cos\alpha)}{D_c} \tag{50}$$

The common denominator D_c is

$$D_c = (\alpha^2 + \alpha\sin\alpha\cos\alpha + \cos 2\alpha - 1) + \bar{I}(\alpha^2 + \alpha\sin\alpha\cos\alpha) \tag{51}$$

As was done before for D_p, the denominator (51) can be expanded for small angles α, with the result here being

$$D_c \cong 2\alpha^2\bar{I}(1 + \alpha^4/45) \equiv 2\alpha^2\bar{I}(1 + 4\lambda^2/15) \tag{52}$$

Appendix II. Radially Loaded Shallow Arch Results

The tangential and radial displacements are found by integrating the shallow arch constitutive equations under appropriate boundary and symmetry conditions, although it is worth noting that the algebra for the shallow arch analysis is far simpler than for the Sanders and Donnell analyzes. For a shallow pinned arch, the exact axial, moment and shear resultants are, respectively

$$N_s^p(\theta) = -N_0 = -qR\left[\frac{8\lambda^2/5}{1 + 8\lambda^2/5}\right] \tag{53}$$

$$M_s^p(\theta) \cong \frac{qL^2/8}{1 + 8\lambda^2/5}(1 - (\theta/\alpha)^2) \tag{54}$$

and

$$Q_s^p(\theta) \cong -\frac{qL/2}{1 + 8\lambda^2/5}\left(\frac{\theta}{\alpha}\right) \tag{55}$$

The corresponding radial displacement is

$$w_s^p(\theta) \cong \frac{\lambda^2/2}{1 + 8\lambda^2/5}\left[5 - 6\left(\frac{\theta}{\alpha}\right)^2 + \left(\frac{\theta}{\alpha}\right)^4\right]\left(\frac{qR^2}{EA}\right) \tag{56}$$

Not surprisingly, Eqs. (54)–(56) are precisely the same as their corresponding small angle results, and Eq. (56) clearly matches the deflection pattern of a uniformly loaded (curved) beam whose value at the crown is exactly that given in Eq. (15).

For the clamped shallow arch, the exact axial, moment and shear resultants are, respectively

$$N_s^c(\theta) = -N_0 = -qR\left[\frac{4\lambda^2/15}{1+4\lambda^2/15}\right] \tag{57}$$

$$M_s^c(\theta) \cong \frac{qL^2/24}{1+4\lambda^2/15}(1-3(\theta/\alpha)^2) \tag{58}$$

and

$$Q_s^c(\theta) \cong -\frac{qL/2}{1+4\lambda^2/15}\left(\frac{\theta}{\alpha}\right) \tag{59}$$

The corresponding radial displacement is

$$w_s^c(\theta) \cong \frac{\lambda^2/2}{1+4\lambda^2/15}\left[1-\left(\frac{\theta}{\alpha}\right)^2\right]^2\left(\frac{qR^2}{EA}\right) \tag{60}$$

Eqs. (58)–(60) are also precisely the same as their foregoing small angle results, and Eq. (60) clearly matches the deflection pattern of a uniformly loaded (curved) fixed-ended beam whose value at the crown is exactly that given in Eq. (23) above. In addition, Eq. (60) is exactly that found in the corresponding prebuckling analysis of a clamped shallow arch [Eq. (3)].

References

Billington, D. P. (1979). *Robert Maillart's bridges: Art of engineering*, Princeton University Press, Princeton, N.J.

Dym, C. L. (1990). *Introduction to the theory of shells*, Hemisphere Publishing, New York.

Dym, C. L. (2002). *Stability theory and its applications to structural mechanics*, Dover, Mineola, N.Y.

Dym, C. L., and Shames, I. H. (1973). *Solid mechanics: Variational approach*, McGraw-Hill, New York.

Heyman, J. (1995). *Stone skeleton: Structural engineering of masonry architecture*, Cambridge University Press, Cambridge, U.K.

Sanders, J. L. (1963). "Nonlinear theories for thin Shells." *Q. Appl. Math.*, 21, 21–36.

Schreyer, H. L., and Masur, E. F. (1966). "Buckling of shallow arches." *J. Engrg. Mech. Div.*, 92(4), 1–19.